ORIGINAL PAPER

R. A. Peters · C. S. Evans

Design of the Jacky dragon visual display: signal and noise characteristics in a complex moving environment

Abstract Visual systems are typically selective in their response to movement. This attribute facilitates the identification of functionally important motion events. Here we show that the complex push-up display produced by male Jacky dragons (*Amphibolurus muricatus*) is likely to have been shaped by an interaction between typical signalling conditions and the sensory properties of receivers. We use novel techniques to define the structure of the signal and of a range of typical moving backgrounds in terms of direction, speed, acceleration and sweep area. Results allow us to estimate the relative conspicuousness of each motor pattern in the stereotyped sequence of which displays are composed. The introductory tail-flick sweeps a large region of the visual field, is sustained for much longer than other components, and has velocity characteristics that ensure it will not be filtered in the same way as wind-blown vegetation. These findings are consistent with the idea that the tail-flick has an alerting function. Quantitative analyses of movement-based signals can hence provide insights into sensory processes, which should facilitate identification of the selective forces responsible for structure. Results will complement the detailed models now available to account for the design of static visual signals.

Keywords Lizards · Movement-based signals · Visual communication · Visual ecology

Introduction

Sensitivity to visual motion helps animals to select functionally-important stimuli for further analysis

R. A. Peters (✉) · C. S. Evans
Animal Behaviour Laboratory, Department of Psychology,
Macquarie University, 2109 Sydney, NSW, Australia
E-mail: richard@galliform.psy.mq.edu.au
Fax: +61-2-98509231

(Nakayama and Loomis 1974). For example, recognition of prey items is much easier when sudden movement compromises crypsis that depends upon appearance (Regan and Beverley 1984), and selective processing of approaching objects facilitates detection of predators (Schiff et al. 1962). However, only a small proportion of environmental movement is relevant. Filtering mechanisms ensure that the limited capacity of the visual system is not overwhelmed by other information.

Considerable progress has been made in explaining the design of static signals. The strategy in such studies has been to combine the objective measurement of structure with knowledge of both the light environment in which the animal is seen, and of sensory processes (Endler 1990, 1992). Selectivity in the response of visual systems to motion is likely to have shaped the evolution of movement-based animal signals in an analogous fashion. In particular, the sensory properties of receivers will define the optimal design for conspicuousness (Guilford and Dawkins 1991; Endler 1992). To convey information effectively, animals must maximise the chance of being detected. This can be achieved by signalling at particular times of the day, when environmental conditions enhance signal intensity (Endler 1991), when receivers' sensory systems are most sensitive (Aho et al. 1988), or when the signals of other species are absent (Greenfield 1988). Each of these strategies effectively increases the signal-to-noise ratio (Endler 1992). The likelihood of detection is also increased if signals contrast with the background against which they are typically performed (Endler 1991; Fleishman 1992). The distinctive colour of some static visual signals facilitates rapid recognition by conspecifics (Bernard and Remington 1991). Similarly, movement-based signals are most effective when they stimulate the visual system in a way that irrelevant visual motion does not (Fleishman 1992).

Direction can be calculated from two relatively imprecise position measurements and is thought to be the first motion variable neurally coded in visual systems (Barlow et al. 1964). The directional selectivity of

individual neurons provides a basic mechanism, which is typically supplemented by integration over a larger population (Grzywacz et al. 1994). Processing of object speed is probably based upon the spatial and temporal properties of directionally selective neuron activity (Simoncelli and Heeger 1998). Direction and speed are fundamental parameters from which other important motion variables (e.g. acceleration) can be derived.

Previous efforts to characterize movement-based lizard signals have used display action patterns to compare the properties of simple movements, such as the head nod (e.g. Martins et al. 1998). These analyses identify differences between display profiles, but only allow weak inferences about the relative conspicuousness of signals. Pioneering work by Fleishman demonstrated the value of a more quantitative approach; comparisons using Fourier analysis show that the displays of *Anolis auratus* have more power at high frequencies than background vegetation movement (reviewed in Fleishman 1992). Similarly, Zeil and Zanker (1997) described the motion characteristics of claw waving in Fiddler crabs (genus *Uca*) using two-dimensional motion detectors to capture the direction and strength of signals in a range of spatio-temporal frequency bands. In a recent paper, we have developed Zeil and Zanker's (1997) idea of using computational motion analysis algorithms to measure the structure of movement-based animal signals (Peters et al. 2002). We used a motion analysis algorithm that estimates velocity based on local changes in image intensity, allowing us to track the direction and speed of movement on a fine temporal scale.

Most previous work on lizard visual signals has focused on displays that are composed of relatively simple, repeated motor patterns. In contrast, the push-up (aggressive) display of the Jacky dragon involves five distinct motor patterns delivered in rapid succession, and subsets of this sequence may be repeated within a display bout. The temporal order of components can be described using Markov chain analysis (e.g. Hailman et al. 1985, 1987), which allows comparisons of gross structure (Peters and Ord 2003). This is a useful first step, but we are particularly interested in the details of signal design. Here we examine the properties of individual display motor patterns, focusing on the degree to which they are each conspicuous against a typical background of wind-blown vegetation.

We used an optic flow algorithm (Peters et al. 2002) to generate 'velocity signatures'—scatterplots representing the direction and speed of movement—for each display component. The shapes of the velocity signatures were then summarised with standard ellipses, which allowed an initial descriptive analysis comparing the signal with background movement. Subsequent analyses sought to specify more precisely how the various sequences differed. First, we collapsed across time to examine direction and speed. Second, direction of movement was ignored to measure variation in speed over time. Finally, we concentrated on the spatial location of motion, ignoring time, direction and speed.

We build upon earlier work describing visual ecology in the context of movement-based signals (Zeil and Zanker 1997; Fleishman 1992). Specifically, our goal was to explain why the tail-flick is used as the introductory component to the push-up display and to identify how constraints imposed by signalling in a complex visual environment might have contributed to the design of this motion-based signal. Detailed description of structural differences between signal components and wind-blown vegetation effectively defines the task faced by the sensory system and should hence provide insights about mechanisms of visual processing in these lizards.

Materials and methods

Apparatus

Video recordings were made using a Canon XL1 digital video camcorder (optical resolution 625 lines) mounted on a tripod. We used a shutter speed of 1/250 s, an aperture of F8 and Sony DVM60EX digital tape (550 lines recorded resolution). The distance between the camera and the subject was constant. Full details of the recording setup for lizard displays are provided in Ord et al. (2002).

Video sequences

Image sequences depicted wind-blown vegetation and the five components of the Jacky dragon push-up display, which were each analysed separately (Fig. 1). Sequence duration was measured in frames at the rate of 25 s^{-1} (PAL standard). Table 1 presents a summary of the sequences used in analyses.

Wind-blown vegetation

Five plant species were selected to represent the habitat in which lizards were originally captured. Species were chosen that typically form the background for basking Jacky dragons: *Acacia longifolia*, *Grevillea linearfolia*, *Kunzea ambigua*, *Pteridium esculentum* and *Xanthorrhea arborea*. Video-recording was carried out in the summer of 2001. We measured wind-speed while filming using a hand-held anemometer (Dick Smith Model Q1411) and obtained sequences of each plant species over the range from 0.70 ms^{-1} to 2.0 ms^{-1}. Analysis of wind-speed data recorded at our field site by the Australian Bureau of Meteorology reveals that this video footage sampled plant movement from light to typical wind conditions (Fig. 2).

Push-up display of the Jacky dragon

We used video footage from an archival collection recorded during a study reported elsewhere (Ord et al. 2002). Each sequence showed a male on a platform made from rough-sawn timber with a uniform and static background. Male Jacky dragon displays consist of a stereotyped series of discrete motor patterns (Fig. 1): introductory tail-flicks are followed by backward and forward arm-waves, a push-up and then a body rock (a wave travelling anterior to posterior down the body). Some, or all, of the components may then be repeated. A total of 53 display sequences from four different male lizards were used in the following analyses of movement characteristics (Table 1). Transition probabilities between display components were calculated from the whole sample.
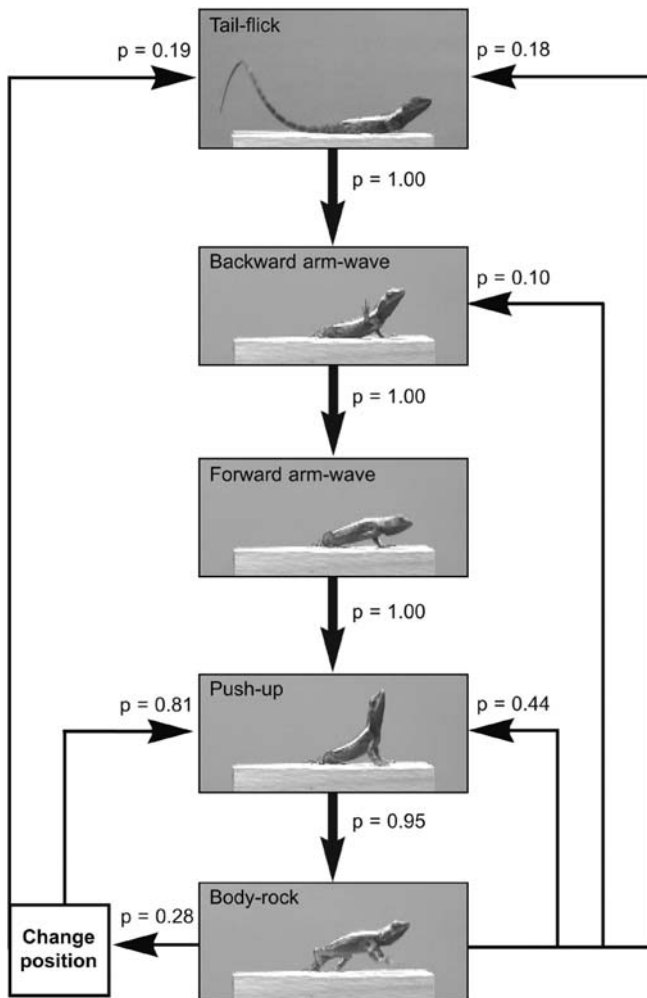
Fig. 1 The push-up display of the Jacky dragon is a stereotyped motor pattern delivered in an obligatory sequence: an introductory *tail-flick* is followed by *backward and forward arm-waves*, and a *push-up*. Displays conclude with a *body-rock*, which is a wave travelling anterior-posterior down the body. These movements can be repeated within a display bout, either from the same spatial location or after a small shift in position and orientation. Transition probabilities are based on Markov chain analysis of 53 sequences (see text for details)

Table 1 Summary of sequences used in analyses

Display component	No. of sequences	Cumulative frame count	Sequence duration (frames)		
			Average	Min.	Max.
Tail-flick	58	2,966	51	26	231
Tail-flick (uncropped)[a]	60	3,203	53	6	148
Backward arm-wave	80	791	10	6	13
Forward arm-wave	81	610	7	5	10
Push-up	152	1,359	9	4	13
Body-rock	137	1,339	10	5	18

[a]See text for details
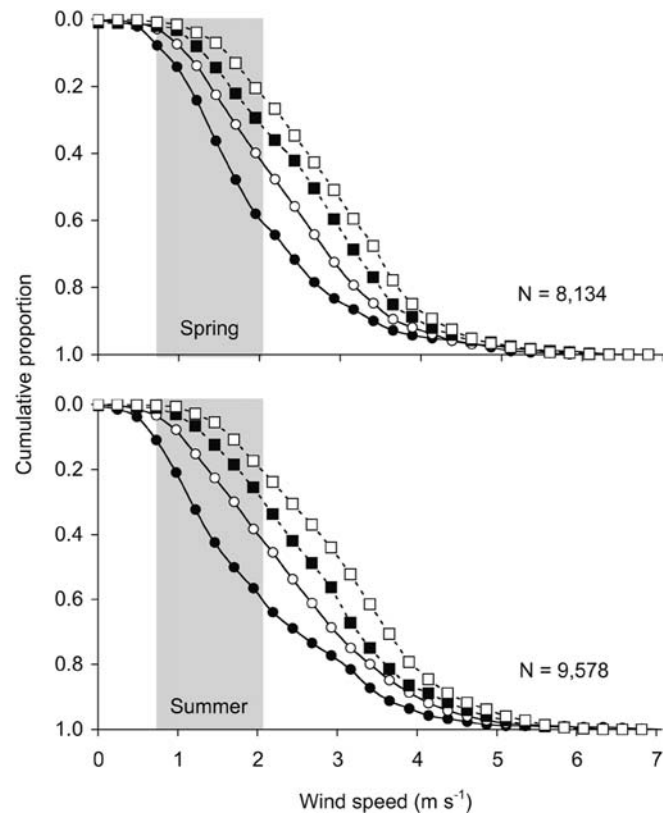
Fig. 2 Distribution of wind-speed measurements during spring (*top*) and summer (*bottom*) for the period 2000–2002. Measurements were taken every 30 min at a height of 10 m and are presented separately for 0800–1000 hours (*solid circles*), 1000–1200 hours (*open circles*), 1200–1400 hours (*solid squares*), 1400–1600 hours (*open squares*). We used the Power-Law (Arya 2001) to estimate wind-speed at the height of our measurements. Recordings taken on overcast days (< 2 h sunshine) were excluded. The *shaded region* indicates the range of wind-speeds for the wind-blown plant sequences in our analyses (source: Australian Bureau of Meteorology)

Computational motion analysis

Our approach for quantifying movement in animal signals, is described in a recent paper (Peters et al. 2002). Briefly, a computational motion analysis algorithm is used to calculate velocity estimates by tracking changes in image intensity. The algorithm assumes a locally constant image structure and calculates the velocity field from temporal and spatial derivatives of filtered versions of image intensity (see Fleet and Langley 1995; Fig. A1 in Peters et al. 2002). Neighbouring locations in natural image sequences tend not to be independent. We therefore combine local measurements of image velocity to obtain a weighted average. This reduces noise to provide a smoothly varying velocity field, while maintaining high spatial resolution. Estimates of movement are calculated over a two-frame window. The spatial distribution of movement can be presented graphically in 'velocity plots' to identify where motion occurs (referred to as optic-flow plots in Peters et al. 2002). Alternatively, we can ignore relative spatial location and present a more concise description of the direction

and magnitude of movement in 'velocity signatures' (Fig. 3a). There are several options available for further analysis, providing summary data that quantify some aspect of the differences between motor patterns. We summarise the general method below, but refer readers to our previous paper (Peters et al. 2002) for technical details.

(a)

(b)

$$\phi^*_{20} = \begin{array}{c} \text{raw angular} \\ \text{deviation} \\ (\theta_{20}) \end{array} - \begin{array}{c} \text{expected angular} \\ \text{deviation of circle} \\ \text{with same radius} \end{array}$$

(c)

(d)

cov = 0.799   cov = 0.005   cov = -0.763

Steps in outline sequence
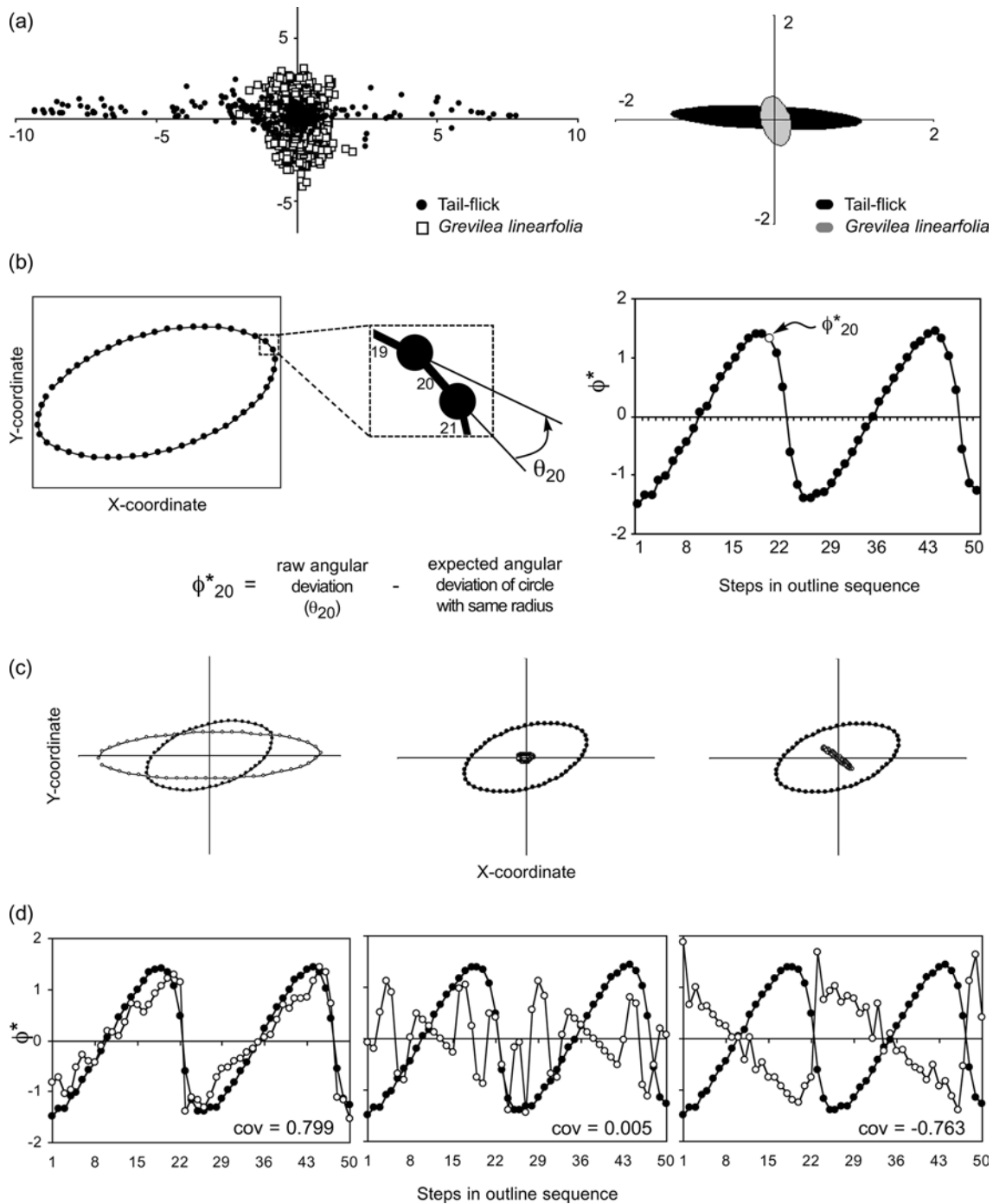
Fig. 3 a The distribution of local velocity estimates generated by the computational motion analysis algorithm can be presented in a velocity signature (*left panel*) and further summarised by a standard ellipse (*right panel*). The Cartesian (*x, y*) form of a standard ellipse can be converted into the Φ* shape function of Zahn and Roskies (1972). This involves interpolation of coordinate pairs, reducing from 197 to 50 in our analysis. **b** We then calculate the net angular deviation between adjacent chords and subtract the expected angular deviation of a circle with the same radius. The first eigenshape of *G. linearfolia* is presented in both Cartesian (**c**) and Φ* forms (**d**). The covariance between individual shape functions and eigenshapes indicates the degree of similarity between outlines. Examples of individual shapes that exhibit high positive, zero, and high negative covariance with the first eigenshape for *G. linearfolia* are shown

General method

Raw footage was transferred digitally from the camcorder to a DraCo non-linear video editing workstation (MS MacroSystem Computer), using an IEEE 1394 'firewire' interface. MovieShop v5.2 software was then used to convert the video clips to sequences of still images, at a rate of 25 s^{-1}. Graphic Converter v3.9.1 software was used to convert images to 8-bit greyscale. To reduce computation time, images were then downsampled to 144×176 pixels.

The motion computation algorithm was implemented using Matlab v5.2.1 for Macintosh and is available from R.A.P. The algorithm calculates estimates of motion for each image point over a two-frame window and represents velocity as separate *x*- and *y*-component vectors. Vector addition of these components

determines the direction and magnitude of velocity at a given image point.

Defining differences between image sequences

In Peters et al. (2002), we presented three approaches for summarising velocity information: calculation of a standard ellipse, response properties of a population of artificially-tuned sensory units, and derivation of a speed-time profile. In the present study, we build upon each of these approaches to explore the relative conspicuousness of Jacky dragon display components.

Standard ellipses and eigenshape analysis

A standard ellipse can be used to summarise movement depicted in a velocity signature (Fig. 3a). This mathematically defines the orientation of movement in the X/Y plane, together with variance in the x and y components, in terms of a shape outline (Batschelet 1981). The analysis of shapes has received detailed consideration in other fields (Dryden and Mardia 1998). We selected eigenshape analysis (Lohmann and Schweitzer 1988; MacLeod 1999), which is analogous to principal components for outline data (Lohmann and Schweitzer 1988; MacLeod 1999). This technique allows us to identify the shapes that explain the most variation in vegetation movement and to examine how each display component compares with these.

First, we determined the standard ellipse for each frame in each sequence. The parametric equation for a standard ellipse requires the mean vector, standard deviations in the x and y planes, and the correlation coefficient (Batschelet 1981). The final parameter is a variable angle increasing in small steps, which are defined manually. We used increments of approximately 1.8° to define the outline in Cartesian (x, y) form using 197 coordinate points.

Second, the Cartesian outline was converted to a mathematical description using the Φ^* (phi*) form of the Zahn and Roskies' (1972) shape function (Fig. 3b). This procedure is fully described by MacLeod (1999). Briefly, it entails (1) interpolating the Cartesian points such that the distance between adjacent points is constant, as well as reducing the number of coordinate pairs (we reduced from 197 to 50 pairs) without any loss of information; (2) calculating the net angular deviation of the chord connecting adjacent coordinate points from the chord connecting the previous set of points; and (3) subtracting the expected net angular change of a circle of the same mean radius to normalise the shape function. This final step is necessary because the parameter of interest in standard eigenshape analysis is the degree to which an outline deviates from a circle (MacLeod 1999).

Third, we performed singular value decomposition (SVD) of the covariance matrix between Φ^* shape functions. This step is conceptually similar to principal components analysis (see Klema 1980), and is useful for identifying important features of a matrix. We calculated a series of orthogonal shape functions (henceforth called eigenshapes), each of which described a percentage of the variance in original shape outlines. Although we calculated all possible eigenshapes for vegetation movement, for simplicity we restricted our analysis to the first two eigenshapes for each vegetation type.

Finally, we calculated the covariance between Φ^* shape functions and the first two eigenshapes of each vegetation type. The covariance between individual shape functions and a particular eigenshape revealed the degree of similarity (Fig. 3c). We can compare the covariance of individual shapes with eigenshapes by plotting covariance scores with one eigenshape against that of another, in eigenshape space. The purpose of these comparisons was to examine how the display components compared with vegetation movement.

Artificial sensory units

Many animals have neurons that exhibit directional selectivity and speed preferences in response to visual stimuli (e.g. lizards: Stein and Gaither 1983; see Introduction). We have emulated this phenomenon by constructing a population of artificial sensory units which process velocity estimates from image sequences (Peters et al. 2002). Differences between movements are revealed in the overall pattern of responses from the population of sensory units, rather than a single summary value. While this artificial system has biologically-plausible properties, we developed it as a new descriptive technique with which to explore the processing of visual motion; it is not an attempt to model the visual system in detail. Briefly, the two-dimensional plane of the velocity signature (Fig. 3a) was the starting point for constructing the sensory units. We divided this space into 16 directions (increments of 22.5°) and added concentric circles to represent three speed classes (3, 6 and 9 pixels per frame). The intersection between each direction and speed determined the preferred velocity of 48 sensory units (Fig. 4a). Gaussian functions defined the response properties within a given speed class, with unit bandwidth increasing with speed (Fig. 4b). All units returned a maximum response of 1 when the observed velocity exactly matched the unit's preferred value. Each sensory unit was presented with all values in the velocity signature.
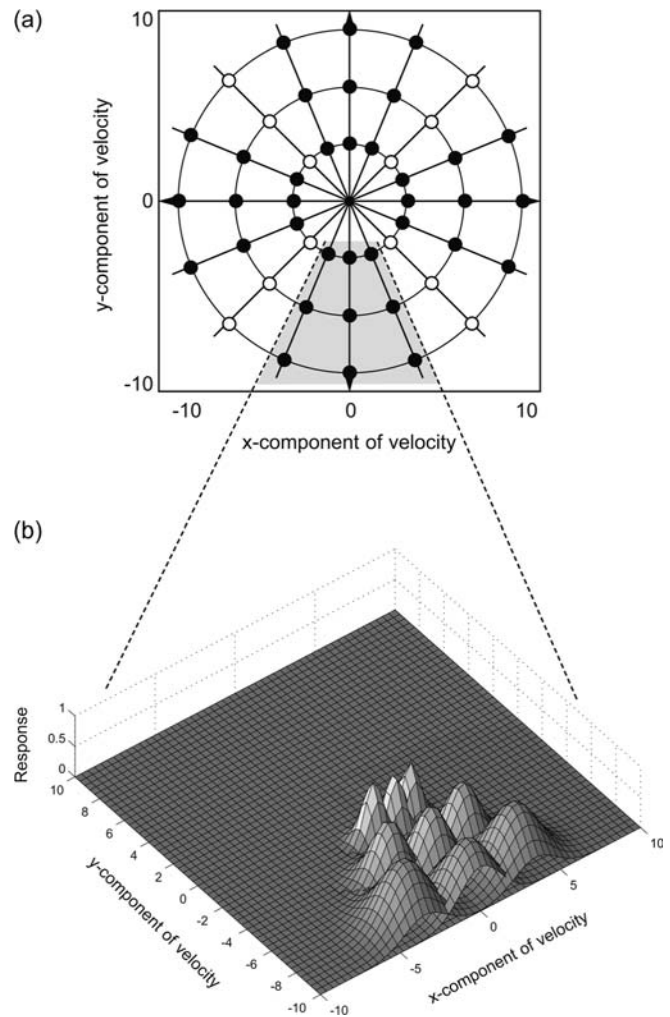
Fig. 4 a Determination of the preferred velocity of 48 artificial sensory units. These form a matrix of 16 directions, with sectors 22.5° wide, by 3 speeds, depicted by concentric circles with radii of 3, 6, and 9 pixels/frame. *Filled circles* represent units used in analyses (see text for details). The *shaded region* is reproduced in **b** to illustrate unit response functions. Sensory unit bandwidth increases with speed, defined by Gaussian functions (SDs of 0.8, 1.3 and 1.8 pixels/frame for slow, moderate and fast units, respectively)

Speed-time profiles

Speed of movement is simply the magnitude of velocity (i.e. vector length). We calculated speed from each velocity estimate by vector addition and application of Pythagoras' theorem. Local speed estimates were then averaged to give an overall movement speed for each frame in each sequence.

Spatial distribution of vectors in velocity plots

We compared the total 'sweep area' for each of the display components by measuring the spatial distribution of velocity estimates. Velocity plots collapsed over time were generated using Matlab v5.2.1 for Macintosh and exported as images. Sweep area was then measured using NIH Object Image v1.62 by drawing a boundary around the region where movement was detected by the algorithm.

Statistical analysis

Standard ellipses were used to obtain a descriptive summary of the velocity estimates depicted in velocity signatures. We analysed vegetation sequences separately for each species to identify the two eigenshapes (or principal components for outline shapes) that explained the greatest variation in movement. The covariance between individual shapes from vegetation sequences and those from each of the five push-up display components was then plotted in eigenshape space.

In the analysis of artificial sensory unit responses, we treated each unit as a separate case and each of the six sequence types as repeated measures variables. We grouped sensory units by speed and direction (Fig. 4). This latter variable was reduced to four classes: up, down, left, and right. Four of the original 16 directions (45°, 135°, 225°, and 315°) lie on the boundary between two classes and were hence excluded. We then compared sensory unit response to sequence types separately within each quadrant and speed class, using Friedman two-way (sensory unit×sequence) analyses of variance by ranks. When significant, these were followed by pair-wise comparisons between each of the display components and vegetation to isolate the sequence types responsible for the overall effect. We identified comparisons where the difference in mean rank exceeded the critical z-value at an alpha level of 0.05, and adjusted for multiple comparisons within speed class ($z_{crit} = 3.50$ for all comparisons; Siegel and Castellan 1988).

For the final two sets of analyses, we averaged across multiple sequences of the same display component type from each lizard to obtain a single individual value (Martin and Bateson 1986). Student's t-tests were then used to compare the speed-time plots from vegetation sequences and lizard display components, with appropriate adjustments for the number of comparisons made to control type I error. Repeated measures ANOVAs were used when comparing between display components; multiple comparisons also used adjusted alpha levels. To examine differences in the spatial distribution of vectors in velocity plots, we compared the sweep area of display components using repeated measures ANOVAs with a single within-subject factor (sequence type). Contrast tests were then conducted between the tail-flick and each of the other components.

Results

Temporal sequence of display components

Jacky dragon push-up displays were delivered in a highly consistent sequence, starting with the tail-flick, followed by the backward and forward arm-waves, the push-up, and the body-rock (Fig. 1). Following the body-rock, the

majority of sequences (67%) repeated from the start of the push-up, either from the same position on the perch (44%) or after a shift in body position ($0.81 \times 0.28 = 23\%$). An alternative pattern involved repetition from the tail-flick component [$0.18 + (0.19 \times 0.28) = 23\%$]. Repetition only rarely occurred from the start of the backward arm-wave (10%), and never from the start of the forward arm-wave.

Standard ellipse and eigenshape analysis

The first two eigenshapes for each foliage type are presented in Fig. 5. The orientation of each eigenshape in
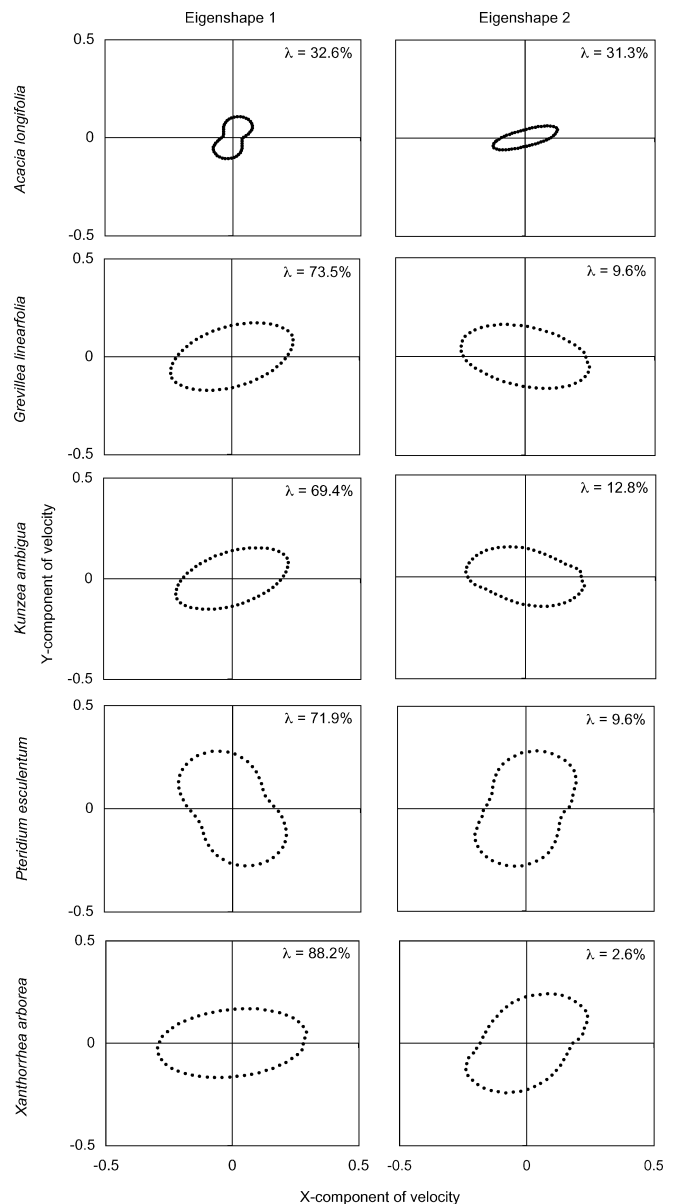
Fig. 5 Outline shapes of the first (*left column*) and second (*right column*) eigenshapes for the five species of vegetation, expressed in Cartesian format. Values (λ) represent the percentage of variance in shape functions explained by each eigenshape

the plot illustrates the direction of movement, and this attribute is the most noticeable difference between the first two eigenshapes for *G. linearfolia, K. ambigua, P. esculentum,* and *X. arborea.* The eigenshapes for *A. longifolia* are tighter around the origin than those of the other plants, revealing less variance in the *x-* and *y-*components (i.e. slower speed) in the original distribution. The eigenshapes for the other four plants show greater speed of movement. The proportion of variance explained by the first eigenshape for *G. linearfolia, K. ambigua, P. esculentum,* and *X. arborea* is relatively high. When a large majority of shape variation is attributed to the first eigenshape, the outlines are said to exhibit a 'fundamental similarity' with each other (MacLeod 1999). This suggests that there is little variation in velocity distributions within each plant species.

Figure 6 presents the covariance between the Φ^* shape functions derived from standard ellipses (Fig. 3) corresponding to each frame of the vegetation sequences and the respective eigenshapes (Fig. 5). As expected *G. linearfolia, P. esculentum,* and *K. ambigua* show positive covariance with the first eigenshape, but little with the second eigenshape. The smaller proportion of vari-

ance explained by the eigenshapes of *A. longifolia* (33% and 31%) is reflected in the eigenshape space. Both positive and negative covariance is observed, but all values are nested against an axis. This suggests that high covariance with one eigenshape is associated with low covariance with the other. In contrast, covariance between the individual shape functions for *X. arborea* and the respective eigenshapes indicates little variation on these two dimensions. This difference in movement characteristics merits further investigation, but, for the purposes of this descriptive analysis, we retain only the first two eigenshapes, which necessarily explain the greatest variation in individual shapes.

The individual Φ^* shape functions of the display components were then compared with the eigenshapes of the vegetation sequences (Fig. 6). These plots indicate that a considerable proportion of the individual shapes generated by each display component sequence are located in a region of eigenshape space not occupied by the vegetation. In comparison to *G. linearfolia, K. ambigua,* and *P. esculentum,* some frames within the display component sequences exhibit positive covariance with both eigenshapes, while others show negative covariance with both. Individual display component shapes appear to show either positive or negative covariance with the first eigenshape of *X. arborea,* rather than no relationship (zero covariance).

In summary, there is a clear difference between the eigenshape space for wind-blown vegetation and that for each of the display components. Based on the shape of

Fig. 6 Covariance between individual shapes (frames) and the first two eigenshapes of each species of vegetation, plotted in eigenshape space. The *left panel* depicts the covariance between individual shapes from the vegetation sequences and their respective eigenshapes. The *remaining panels* present the covariance between display component shapes and the eigenshapes for each vegetation movement
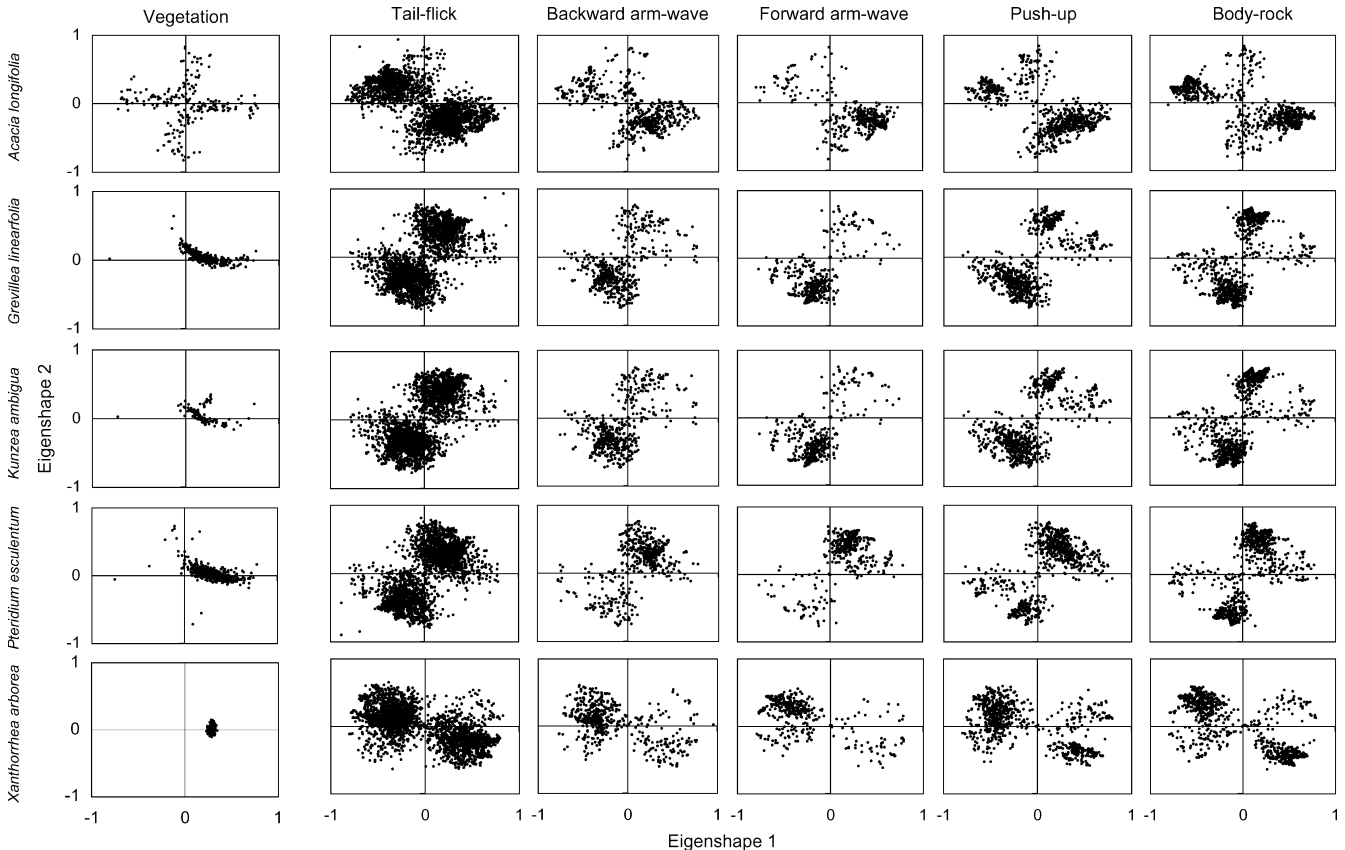
the velocity distribution, each motor pattern is thus structurally distinct from background movement.

Artificial sensory units

Figure 7 summarises the responses of sensory units to each sequence type. Vegetation movement accounted for most of the activity in sensory units tuned to slow speeds (Fig. 7, top). In contrast, units tuned to moderate and fast speeds responded principally to display components (Fig. 7, middle and bottom).

For sensory units tuned to slow speed, Friedman ANOVAs were significant for movement upwards ($X^2 = 13.5$, df = 5, p = 0.019), downwards ($\chi^2 = 14.6$, df = 5, p = 0.012), and to the left ($X^2 = 14.6$, df = 5, P = 0.012), but not to the right ($X^2 = 9.6$, df = 5, P = 0.079). Pair-wise comparisons ($z_{crit} = 3.50$, adjusted for the number of comparisons) reveal that this difference reflects greater sensitivity to vegetation movement. Units tuned to upward movement responded significantly more toward vegetation than the backward arm-wave

Fig. 7 Response of sensory units to display components, averaged by direction and speed of movement. Values represent the response to display components minus the response to vegetation movement. Positive values thus indicate greater response to displays. Note that the range of values depicted differs between speed classes to accommodate the much larger absolute level of sensory unit activity at slow speeds. *Stars* indicate significant differences between display components and vegetation. *TF* tail-flick, *BAW* backward arm-wave; *FAW* forward arm-wave; *PU* push-up; *BR* body-rock

(mean ranks of 5.33 and 1.00, respectively), while units tuned to downward movement responded more to vegetation than both the backward arm-wave (6.00 versus 2.00) and the forward arm-wave (6.00 versus 1.00). These results suggest that display components were effectively masked at slow speeds.

All Friedman tests for sensory units tuned to moderate speeds were significant (up: $X^2 = 12.3$, df = 5, P = 0.03; right: $X^2 = 13.1$, df = 5, P = 0.023; down: $X^2 = 12.9$, df = 5, P = 0.024; and left: $X^2 = 14.6$, df = 5, P = 0.012). Pair-wise comparisons were conducted using the same criterion as above ($z_{crit} = 3.50$). The body-rock (mean rank of 5.67) and push-up (5.33) elicited greater responses than vegetation (1.67) for units tuned to movement right, while the body-rock (6.00) and tail-flick (5.00) elicited greater responses for movement left than vegetation (1.33).

Friedman tests for units tuned to fast speeds were also all significant (up: $X^2 = 13.5$, df = 5, P = 0.019; right: $X^2 = 13.9$, df = 5, P = 0.017; down: $X^2 = 13.1$, df = 5, P = 0.023; and left: $X^2 = 13.5$, df = 5, P = 0.019). Response to the body-rock was significantly different ($z_{crit} = 3.50$) from vegetation in units tuned to movement up (mean ranks of 6.00 versus 2.00), right (5.67 versus 1.33) and left (6.00 versus 1.00). Response to the push-up (5.33) was also significantly greater than vegetation (1.33) for movement to the right, while the forward arm-wave (4.67) exceeded vegetation (1.00) for movement to the left.

This pattern of results suggests that some display components have velocity characteristics quite different from those of vegetation and identifies the speed-orien-

tation attributes principally responsible for structural conspicuousness.

Speed-time profiles

We calculated the average speed of movement in successive frames of all sequences. The speed-time profiles of representative tail-flick, body-rock, and wind-blown vegetation are shown in Fig. 8a. Both the tail-flick and body-rock generate rapidly changing profiles, in contrast to the almost constant profile of the vegetation sequence. To test whether these differences were statistically significant, we first calculated the difference in speed between consecutive frames and then averaged the absolute value of these changes within each sequence (Fig. 8b). A one-way ANOVA revealed that there were no significant differences among the vegetation sequences after they were log_{10} transformed to eliminate positive skew [$F_{(4,59)} = 2.41$, $P > 0.05$], so we pooled these data. Pair-wise comparisons show that each display component had significantly greater frame-to-frame speed changes than the average of vegetation sequences (tail: $T = 11.1$, $df = 5$; $P < 0.001$; backward arm-wave:

$T = 9.5$, $df = 5$; $P < 0.001$; forward arm-wave: $T = 6.3$, $df = 5$; $P < 0.01$; push-up: $T = 11.$, $df = 5$; $P < 0.001$; body-rock: $T = 7.8$, $df = 5$, $P < 0.001$).

We also compared the speed characteristics of each of the display components. A repeated measures ANOVA revealed a significant overall effect for movement type [$F_{(4,12)} = 11.3$, $P < 0.001$]. Multiple comparisons showed that the push-up had significantly greater acceleration/deceleration values than the tail-flick and backward arm-wave ($P = 0.018$ and $P = 0.021$, respectively); no other comparisons were significant.

A final analysis was designed to estimate the relative conspicuousness of display components in terms of speed. To be conservative, we used the fastest movement observed in vegetation sequences—thus simulating detectability under the most adverse signalling conditions that we measured. We calculated the number of frames in each display sequence that exceeded the observed maximum speed measured from each of the five vegetation sequences separately and then averaged within each lizard for each motor pattern (Fig. 8c). A repeated-measures ANOVA revealed main effects for both display component [$F_{(4,12)} = 79.0$, $P < 0.001$] and vegetation type [$F_{(4,12)} = 42.3$, $P < 0.001$], as well as a

Fig. 8 a Speed-time profiles for representative tail-flick, body-rock, and vegetation sequences. **b** Mean (+SE) difference in speed between successive frames of the display component and that of pooled vegetation sequences. **c** Mean (+SE) number of frames per sequence (*bars*) and mean (±SE) proportion of sequence (*line*) in which the speed of display movements exceeded the maximum value measured in any vegetation sequence. *TF* tail-flick, *BAW* backward arm-wave; *FAW* forward arm-wave; *PU* push-up; *BR* body-rock; *V* vegetation
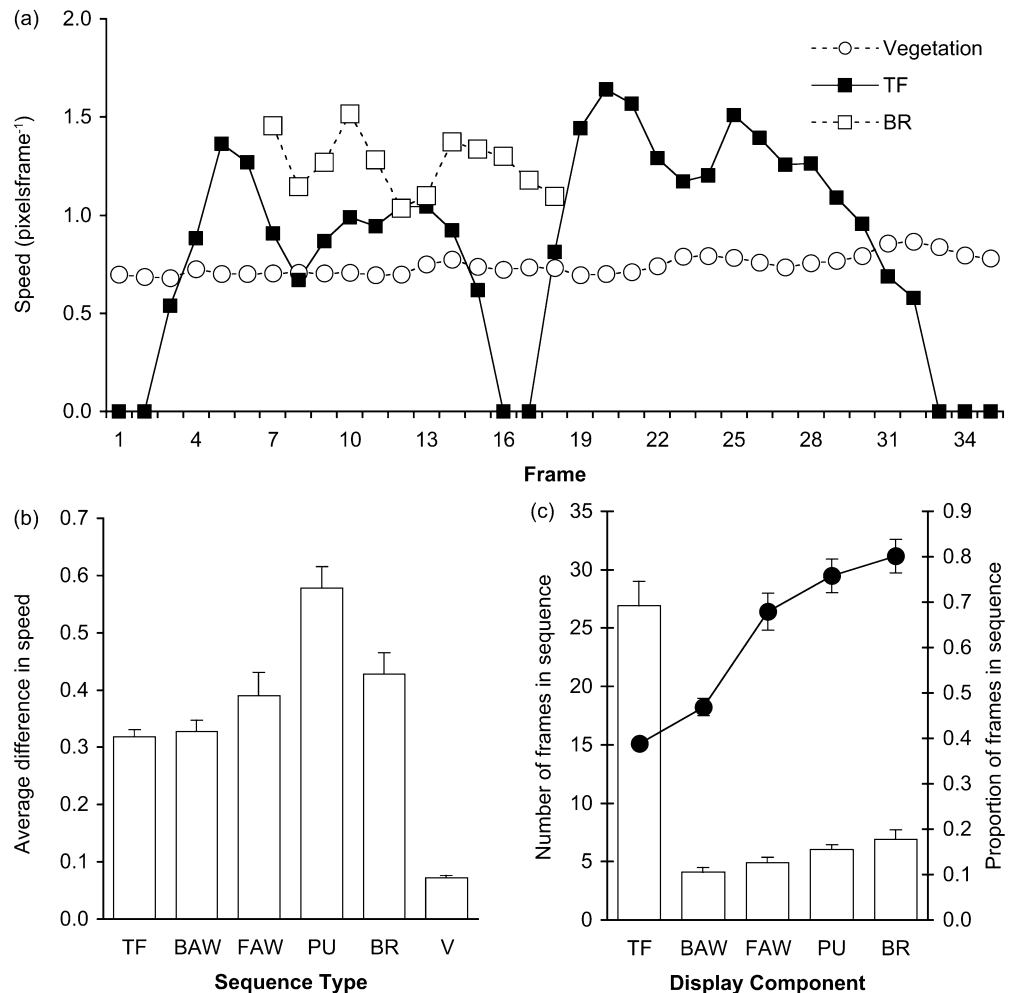
significant interaction [$F_{(16,48)} = 23.6$, $P < 0.001$]. Subsequent comparisons between individual display components and vegetation sequences show that the main effect for movement type was attributable to the tail-flick. The number of frames in tail-flick sequences exceeding maximum vegetation speed was significantly greater than in any of the other display components ($P < 0.05$ for each comparison); no other comparisons between display components were significant.

There is an approximately fivefold difference in duration between the tail-flick and the other display components (Table 1), suggesting that the much higher scores for this introductory component (Fig. 8c) might reflect sequence length, rather than structure. We therefore conducted a complementary analysis in which the number of frames exceeding maximum vegetation speed was expressed as a proportion of sequence length. Both main effects remained significant [display component: $F_{(4,12)} = 20.4$, $P < 0.01$; vegetation type: $F_{(4,12)} = 36.6$, $P < 0.01$], but the interaction was no longer significant. The function depicting this estimate of structural conspicuousness (Fig. 8c; line) increases linearly over the course of a typical display from the tail-flick to the body-rock [$F_{(1,3)} = 114.6$, $P < 0.001$]. No multiple comparisons for the vegetation type main effect were significant after adjusting for the number of comparisons.

Spatial distribution in velocity plots

The spatial distribution of movement in a velocity plot defined the relative sweep area of display components (Fig. 9a). A repeated-measures ANOVA with the single factor of display component type was marginally non-significant after adjusting the degrees of freedom due to violation of the assumption of sphericity [$F_{(4,12)} = 7.169$, $P < 0.07$]. It seemed likely that this result reflected constraints in our original video-recording setup. We used archival footage of lizards displaying on an artificial perch (see Materials and methods), which had been filmed so that animals appeared life-sized on the video monitor subsequently used for playback presentations (Ord et al. 2002). This meant that several tail flick sequences were cropped (i.e. the most distal section occasionally moved out of the camera field). This was not a problem with any of the other display movements. We added additional tail-flick sequences from the same lizards (Table 1) in which they were not restricted to displaying on the artificial perch, but which included other objects of known size, and generated velocity plots adjusted to scale. The inclusion of uncropped sequences now revealed considerable variation between components in average sweep area (Fig. 9b) and the corresponding ANOVA was significant [$F_{(4,12)} = 10.175$, $P = 0.012$]. Pairwise comparisons between display movements show that the sweep area of the tail-flick was significantly greater than that of the backward arm-wave [$F_{(1,3)} = 22.244$, $P = 0.018$]. Tests comparing the tail-flick
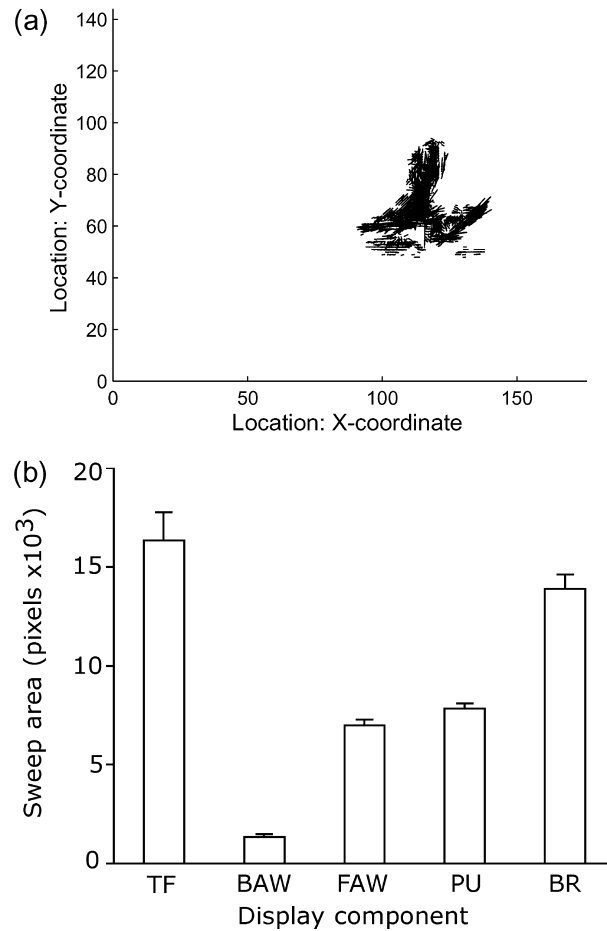
Fig. 9 a Velocity plot of a representative push-up. Sweep area is calculated by tracing around the region occupied by individual vectors (see text for details). **b** Average ($+$SE) sweep area for each display component type. *TF* tail-flick, *BAW* backward arm-wave; *FAW* forward arm-wave; *PU* push-up; *BR* body-rock

with both the forward arm-wave and the push-up also approached significance [$F_{(1,3)} = 8.065$, $P = 0.066$ and $F_{(1,3)} = 7.877$, $P = 0.067$, respectively].

Discussion

Structure of signal and noise

The five components of the push-up display were described in terms of direction and speed of movement, and these characteristics were compared to those of wind-blown vegetation against which signals would typically be seen. We focused particularly on why the tail-flick is used as the introductory display component, comparing this motor pattern with those that follow it to assess conspicuousness relative to background movement. We first defined the structure of background noise using eigenshape analysis (Figs. 3 and 5) and then calculated the covariance between these shapes and those generated by display motor patterns. There was little similarity between the signal and background noise in

terms of the distribution of velocity estimates (Fig. 6). This initial analysis thus revealed that there are reliable structural differences between wind-blown vegetation movement and display motor patterns.

We then used three complementary analytical approaches to elucidate the nature of these differences. First, we collapsed across time to examine direction and speed of movement, using a population of velocity-tuned sensory units (Fig. 4; Peters et al. 2002). Results suggest that units tuned to slow speeds would be excited principally by wind-blown vegetation, irrespective of direction (Fig. 7, top). However, units with moderate and fast speed preferences would readily detect each component of the display, except the backward arm-wave, against background noise (Fig. 7, middle and bottom).

Second, we ignored direction and considered variation in speed over time (Fig. 8). All display motor patterns had significantly higher acceleration/deceleration than those obtained from the relatively smooth speed-time profile of wind-blown vegetation (Fig. 8b). This finding supports those from Fleishman's (1988a) Fourier analyses of *Anolis* lizard displays and background. We also extend this earlier work by assessing relative conspicuousness of display components with direct measurements of movement speed. To be conservative, we used the maximum speed of vegetation sequences in our recordings as the reference value. The tail-flick exceeds other display components by a factor of 3–6 when number of frames with speed greater than background is used as the unit of measurement (Fig. 8c, bars). However, this effect is largely a product of movement duration (Table 1). When speed differences are expressed using a proportion of frames (Fig. 8c, line), the display actually increases in structural conspicuousness from the tail-flick through to the body-rock (Fig. 8c, line). This interaction between component duration and speed is particularly important in the context of signal design, which we discuss below.

Finally, we considered the region in which motion occurred, by defining the sweep area of each component (Fig. 9). This analysis suggested that the tail-flick and the body-rock cover the largest area of the visual field.

The present study is an initial step in the exploration of Jacky dragon signal design. To make analyses more tractable, it was necessary to reduce the number of variables by fixing some parameters. Specifically, we examined the relative conspicuousness of display components at the same viewing distance as plant movement, and during light to typical wind conditions (Fig. 3). To understand fully the effect of environmental conditions on these signals, it will be useful to quantify plant movement during stronger winds, and to obtain information about the actual conditions in which displays occur. We plan also to investigate the effects of variation in viewing distance. Attributes such as sweep area (expressed as a proportion of the visual field) will change predictably as a function of the separation between sender and receiver. In addition, vegetation movement will not typically occur in the same plane as

the signal, but rather over a range of distances, with correlated variation in perceived amplitude. We anticipate that there will therefore be complex interactions between signal and noise characteristics once viewing distance is taken into account. Understanding these relationships will be important for developing more sophisticated models of the recognition of movement-based signals.

Mechanisms of visual processing

Analyses of typical natural scenes reveal highly constrained spatial statistics (e.g. Field 1987). Complementary descriptions of the temporal structure of typical image streams, as perceived by the animal's visual system, are presented in terms of the movement of the animal itself, and similarly feature statistics that are predictable and redundant (van Hateren 1992b). It has been suggested that early visual processing can reduce the redundancy in natural scenes (e.g. Barlow 1961; Srinivasan et al. 1982), or enhance it to maximise the transfer of spatiotemporal information through noisy channels of limited capacity, thus increasing signal reliability (e.g. van Hateren 1992a, 1992b). However, these descriptions largely ignored less frequent, but nonetheless functionally-important tasks of visual processing (Zeil and Zanker 1997). The present analysis is one step toward the goal of understanding the visual ecology of an animal that relies on motion cues in contexts such as detecting predators, identifying prey items, and interacting with conspecifics. If we consider the motion analysis algorithm used in the present study as being broadly analogous to early visual processing, then the output defines the spatiotemporal information available to higher order visual processes.

For sit-and-wait predators like the Jacky dragon, as well as many other non-mammalian vertebrates, the optic tectum is responsible for selective orientation to relevant environmental events (Ulinski et al. 1992; Fleishman 1992; Persons et al. 1999). Animals are also capable of responding in a graded fashion. These observations suggest that some stimulus evaluation is occurring during the earliest stages of visual processing. For example, Fleishman (1986) demonstrated that lures with square-wave motion patterns (i.e. rapid changes in speed) were more effective at eliciting orienting responses in lizards (Genus: *Anolis)* than lures with a smooth, sinusoidal motion pattern.

There is considerable evidence that visual systems select sub-sets of stimuli for further processing based on the direction and speed of movement (Barlow et al. 1964; Sekular 1990; Ibbotson et al. 1994; Cheng et al. 1994). Cells within the optic tectum of the lizard *Iguana iguana* have been shown to exhibit both directional selectivity, and a preference for particular speeds (Stein and Gaither 1983). The relative response of directionally selective cells in the optic tectum hence provides a possible mechanism for assessing differences among visual

motion cues. The response properties of our artificial sensory units illustrate one way in which a visual system might process activity from a population of motion-sensitive cells. Signal movements were most conspicuous to sensory units with moderate to fast speed preferences, while those tuned to slower speeds would likely be habituated because of constant stimulation from background vegetation movement.

Our analysis of sensory unit responses considered movement characteristics in terms of direction and speed, but ignored variation over time by using a single summary value. Complementary analyses of speed-time profiles suggest that temporal changes in visual motion could provide enhanced discrimination of signal from noise. The most notable feature of the speed-time profiles (Fig. 8) is the contrast between the rapid acceleration/deceleration of display components, and the almost invariant movement of vegetation (see also Fleishman 1988a). This suggests that if temporal differences in the response of units were being computed, orienting to relevant cues could occur even at speeds that are, on average, less than background noise.

The visual system would also need to achieve translation-invariance, particularly at the level of analysis required for orienting responses. A parsimonious solution would be to use differences in relative speed to segregate motion events in the environment. Monitoring the temporal properties of directionally selective cells, as described above, might be satisfactory. Alternative explanations have been proposed, which suggest that calculations of speed, independent of direction and position (Sekular 1990), or the response of cells sensitive to adjacent areas moving at different speeds (Orban et al. 1987), might also be mechanisms for segregating visual input.

Conspicuousness and signal design

Our results demonstrate that each component of the display is structurally conspicuous against a typical moving background. However, this attribute is not sufficient to explain fully signal design. Jacky dragon displays invariably begin with a tail-flick (Fig. 1), which has the likely function of attracting the attention of receivers. Alerting signals typically have simple structure, high intensity, and short duration (Fleishman 1988b; Richards 1981). For example, the lizard *Anolis auratus* uses large-amplitude head movements to generate the high velocity and acceleration necessary for engaging the visual grasp reflex of an opponent (Fleishman 1988a). We suggest that the tail-flick may achieve a similar result, but in a different way. While the tail-flick appears less intense than other display components when speed is expressed as a proportion of frames exceeding maximum vegetation value, it has the highest absolute score because its duration is qualitatively greater than that of any other movement (Fig. 8c).

The probability of attracting the attention of conspecifics in the visual domain is constrained by receiver orientation; even the most intense signal cannot be detected if it is outside the visual field. Adaptations such as laterally placed eyes, which increase the field of view (Moermond 1981), and a high concentration of motion-sensitive cells in the periphery (Stein and Gaither 1983), increase the likelihood of detecting salient visual motion. Nevertheless, constant scanning of the environment is necessary to obtain full coverage of the visual field, and this behaviour is characteristic of our subjects. Signals with a long duration and a large sweep area (Fig. 9), will therefore have the best chance of being detected. Playback experiments (e.g. Ord et al. 2002) are planned to test the prediction that displays preceded by the tail-flick will be more conspicuous than others edited to lack this component.

It would also be interesting to conduct comparative analyses of the structure of visual alerting signals. The contrast between the introductory components of the Jacky dragon display and that of *A. aurutus* suggest that there are several possible solutions to the design problem of attracting receiver attention. We speculate that this diversity might reflect an energetic trade off between movement intensity and duration.

Our approach will also allow exploration of the way in which different habitat types have affected signal design—for example, testing the prediction that higher energy displays are needed for densely vegetated areas (Fleishman 1992). Findings will complement what is already known about the role of brightness contrast and spectral sensitivity in shaping the design of movement-based animal signals (e.g. Leal and Fleishman 2002; Fleishman et al. 1997).

References

Aho A-C, Donner K, Hyden C, Larsen LO, Reuter T (1988) Low retinal noise in animals with low body temperature allows high visual sensitivity. Nature 334:348–350

Arya SP (2001) Introduction to Micrometeorology. Academic Press, San Diego, CA

Barlow HB (1961) Possible principles underlying the transformations of sensory messages. In: Rosenblith WA (ed) Sensory communication. MIT Press, Cambridge, MA

Barlow HB, Hill RM, Levick WR (1964) Retinal ganglion cells responding selectively to direction and speed of image motion in the rabbit. J Physiol (Camb) 173:377–407

Batschelet E (1981) Circular statistics in biology. Academic Press, London

Bernard GD, Remington CL (1991) Color vision in *Lycaena* butterflies: spectral tuning of receptor arrays in relation to behavioral ecology. Proc Natl Acad Sci USA 88:2783–2787

Cheng K, Hasegawa T, Saleem KS, Tanaka K (1994) Comparison of neuronal selectivity for stimulus speed, length, and contrast in the prestriate visual cortical areas V4 and MT of the Macaque monkey. J Neurophysiol 71:2269–2280

Dryden IL, Mardia KV (1998) Statistical shape analysis. Wiley, Chichester, UK

Endler JA (1990) On the measurement and classification of colour in studies of animal colour vision. Biol J Linn Soc 41:315–352

Endler JA (1991) Variation in the appearance of guppy color patterns to guppies and their predators under different visual conditions. Vision Res 31:587–608

Endler JA (1992) Signals, signal condition and the direction of evolution. Am Nat 139:125–153

Field DJ (1987) Relations between the statistics of natural images and the response properties of cortical cells. J Opt Soc Am A 4:2379–2394

Fleet DJ, Langley K (1995) Recursive filters for optic flow. IEEE Transactions on Pattern Analysis and Machine Intelligence 17:61–67

Fleishman LJ (1986) Motion detection in the presence or absence of background motion in an *Anolis* lizard. J Comp Physiol A 159:711–720

Fleishman LJ (1988a) Sensory and environmental influences on display form in *Anolis auratus*, a grass anole of Panama. Behav Ecol Sociobiol 22:309–316

Fleishman LJ (1988b) Sensory influences on physical design of a visual display. Anim Behav 36:1420–1424

Fleishman LJ (1992) The influence of the sensory system and the environment on motion patterns in the visual displays of anoline lizards and other vetebrates. Am Nat 139 [Suppl]:S36–S61

Fleishman LJ, Bowman M, Saunders D, Miller WE, Rury MJ, Loew ER (1997) The visual ecology of Puerto Rican anoline lizards: habitat light and spectral sensitivity. J Comp Physiol A 181:446–460

Greenfield MD (1988) Interspecific acoustic interactions among katydids *Neoconocephalus*: inhibition-induced shifts in diel periodicity. Anim Behav 36:684–695

Grzywacz NM, Harris JM, Amthor FR (1994) Computational and neural constraints for the measurement of local visual motion. In: Smith AT, Snowden RJ (eds) Visual detection of motion. Academic Press, London, pp 19–50

Guilford T, Dawkins MS (1991) Receiver psychology and the evolution of animal signals. Anim Behav 42:1–14

Hailman JP, Ficken MS, Ficken RW (1985) The 'chick-a-dee' calls of *Parus atricapillus*: a recombinant system of animal communication compared with written English. Semiotica 56:191–224

Hailman JP, Ficken MS, Ficken RW (1987) Constraints on the structure of combinatorial 'chick-a-dee" calls. Ethology 75:62–80

Hateren JH van (1992a) Real and optimal neural images in early vision. Nature 360:68–70

Hateren JH van (1992b) Theoretical predictions of spatiotemporal receptive fields of fly LMCs, and experimental validation. J Comp Physiol A 171:157–170

Ibbotson MR, Mark RF, Maddess TL (1994) Spatiotemporal response properties of direction-selective neurons in the optic tract and dorsal terminal nucleus of the wallaby, *Macropus eugenii*. J Neurophysiol 72:2927–2943

Klema VC (1980) The singular value decomposition: its computation and applications. IEEE Transaction on Automatic Control 25:164–176

Leal M, Fleishman LJ (2002) Evidence for habitat partitioning based on adaptation to environmental light in a pair of sympatric lizard species. Proc R Soc Lond Ser B 269:351–359

Lohmann GP, Schweitzer PN (1988) On eigenshape analysis. In: Rohlf FJ, Bookstein FJ (eds) Proceedings of the Michigan Morphometrics Workshop. University of Michigan Museum of Zoology, Ann Arbor, pp 147–166

MacLeod N (1999) Generalizing and extending the eigenshape method of shape space visualization and analysis. Paleobiology 25:107–138

Martin P, Bateson P (1986) Measuring behaviour. Cambridge University Press, Cambridge

Martins EP, Bissell AN, Morgan KK (1998) Population differences in a lizard communicative display: evidence for rapid change in structure and function. Anim Behav 56:1113–1119

Moermond TC (1981) Prey-attack behavior of *Anolis* lizards. Z Tierpsychol 56:128–136

Nakayama K, Loomis JM (1974) Optical velocity patterns, velocity-sensitive neurons, and space perception: a hypothesis. Perception 3:63–80

Orban GA, Gulyas B, Vogels R (1987) Influence of a moving textured background on direction selectivity of cat striate neurons. J Neurophysiol 57:1792–1812

Ord TJ, Peters RA, Evans CS, Taylor AJ (2002) Digital video playback and visual communication in lizards. Anim Behav 63:879–890

Persons MH, Fleishman LJ, Frye MA, Stimphil ME (1999) Sensory response patterns and the evolution of visual signal design in anoline lizards. J Comp Physiol A 184:585–607

Peters RA, Ord T J (2003) Display response of the Jacky dragon, *Amphibolurus muricatus* (Lacertilia: Agamidae), to intruders: a semi-Markovian process. Austral Ecol (in press)

Peters RA, Clifford CWG, Evans CS (2002) Measuring the structure of dynamic visual signals. Anim Behav 64:131–146

Regan D, Beverley KI (1984) Figure-ground segregation by motion contrast and by luminance contrast. J Opt Soc Am A 1:433–442

Richards DG (1981) Alerting and message components in songs of rufous-sided towhees. Behaviour 76:223–249

Schiff W, Caviness JA, Gibson JJ (1962) Persistent fear responses in Rhesus monkeys to the optical stimulus of "looming". Science 136:982–983

Sekular AB (1990) Motion segregation from speed differences: evidence for nonlinear processing. Vision Res 30:785–795

Siegel S, Castellan NJ (1988) Nonparametric statistics for the behavioural sciences. McGraw-Hill, New York

Simoncelli EP, Heeger DJ (1998) A model of neuronal responses in visual area MT. Vision Res 38:743–762

Srinivasan MV, Laughlin SB, Stavenga DG (1982) Predictive coding: a fresh view of inhibition in the retina. Proc R Soc Lond Ser B 216:427–459

Stein BE, Gaither NS (1983) Receptive-field properties on reptilian optic tectum: some comparisons with mammals. J Neurophysiol 50:102–124

Ulinski PS, Dacey DM, Sereno MI (1992) Optic tectum. In: Gans C, Ulinski PS (eds) Biology of the Reptilia, vol 17. Neurology C, sensorimotor integration. University of Chicago Press, Chicago, pp 241–366

Zahn CT, Roskies RZ (1972) Fourier descriptors for plane closed curves. IEEE Transactions on Computers c-21:269–281

Zeil J, Zanker JM (1997) A glimpse into crabworld. Vision Res 37:3417–3426